Journal of Metals, Materials and Minerals, 36(3), e2597, 2026

Synergistic adsorption–photocatalysis of activated carbon/titanium dioxide composite derived from rice husk ash under ultraviolet-C irradiation

Bang-Tam Thi DAO[1,2,*], Do Trung NGUYEN[1,2], Nhien Hon LE[1,2] and Chi-Nhan HA-THUC[1,2,*]

[1] *Faculty of Materials Science and Technology, University of Science, Ho Chi Minh City, Vietnam – 227 Nguyen Van Cu Street, Cho Quan Ward, Ho Chi Minh City, 700000, Vietnam*

[2] *Vietnam National University, Ho Chi Minh City, Vietnam – Vo Truong Toan Street, Linh Xuan Ward, Ho Chi Minh City, 700000, Vietnam*

***Corresponding author e-mail**: htcnhan@hcmus.edu.vn; dtbtam@hcmus.edu.vn

Received date:
5 December 2025
Revised date:
23 December 2025
Accepted date:
21 May 2026

Keywords:
Activated carbon;
Rice husk ash;
Titanium dioxide;
Dye degradation;
Water treatment

Abstract

Rice husk ash (RHA), an abundant biomass residue, was employed as a sustainable precursor for synthesizing activated carbon (AC) and its TiO_2-based photocatalyst composite. AC was produced via ultrasonication-assisted NaOH activation of KOH-impregnated biochar, yielding a highly porous material with a large surface area. Titanium dioxide nanoparticles were synthesized from titanium (IV) isopropoxide (TTIP) and subsequently immobilized onto AC to form the AC/TiO_2 composite. Structural and textural analyses (XRD, FT-IR, BET, SEM–EDS) confirmed the presence of anatase TiO_2 uniformly distributed within the AC framework while preserving its porous architecture. The photocatalytic activity of the composite was assessed using Basic Blue 3 (BB3) as a model dye under UVC irradiation. Whereas pristine AC removed ~85% of BB3 primarily through adsorption, the AC/TiO_2 composite achieved up to 98% removal within 120 min due to the synergistic contribution of adsorption and photocatalysis. GC–MS analysis revealed that AC/TiO_2 not only decolorized the dye but also induced extensive molecular fragmentation, including cleavage of azo bonds and aromatic ring opening, confirming genuine photocatalytic degradation beyond surface adsorption. Overall, the biomass-derived AC/TiO_2 composite demonstrates strong potential as an efficient and sustainable photocatalyst for dye-contaminated wastewater treatment.

1. Introduction

Water pollution caused by persistent organic contaminants, particularly synthetic dyes released from textile industries, remains a pressing global environmental concern [1,2]. These dyes are not only resistant to natural degradation but also pose significant risks to aquatic ecosystems and human health due to their toxicity and potential mutagenicity [3,4]. Conventional wastewater treatment methods, including coagulation, adsorption, and biological processes, often fail to achieve complete mineralization of these compounds [5,6]. Therefore, the development of advanced, sustainable, and cost-effective treatment technologies is urgently needed.

Among the available advanced oxidation processes (AOPs), photocatalysis has emerged as a promising approach due to its ability to generate reactive oxygen species capable of degrading a wide range of organic pollutants into harmless end products [7,8]. Titanium dioxide (TiO_2) is one of the most extensively studied photocatalysts because of its high stability, strong oxidation ability, low toxicity, and cost-effectiveness [9,10]. However, pristine TiO_2 suffers from certain drawbacks, including rapid recombination of photogenerated electron–hole pairs and limited visible-light response, which reduce its overall photocatalytic efficiency [11,12].

To address these limitations, recent research has focused on the modification of TiO_2 with various supports and dopants [13]. Activated carbon (AC), with its high surface area, tunable porosity, and abundant functional groups, has been widely employed as a support material for TiO_2 [14,15]. The synergistic effect between the adsorption capability of AC and the photocatalytic activity of TiO_2 facilitates the concentration of pollutants near active sites and prolongs charge separation, thereby enhancing degradation efficiency [16,17]. Moreover, utilizing biomass-derived precursors to produce AC provides an additional environmental benefit by valorizing agricultural waste [18].

Rice husk, an abundant byproduct of rice production, represents a sustainable feedstock for synthesizing AC due to its high carbon and silica content [19]. The conversion of rice husk into AC not only offers a low-cost material with excellent adsorption capacity but also addresses the issue of agricultural waste disposal [20]. Unlike conventional biomass-derived activated carbons that typically require high-temperature pyrolysis or thermal activation, the present study employs a combined NaOH–ultrasonication activation strategy without an additional pyrolysis step. Despite the mild processing conditions, the obtained activated carbon exhibited a highly porous structure and large specific surface area, providing an effective support for TiO_2 dispersion and synergistic adsorption–photocatalytic degradation.

In this study, we report the synthesis of a rice husk–derived AC/TiO_2 nanocomposite and its application in photocatalytic degradation of a model organic dye under UVC irradiation. Comprehensive physicochemical characterizations, including XRD, FT-IR, BET, and SEM–

EDS, were performed to elucidate the structural and morphological features of the composite. The photocatalytic performance was evaluated and compared with pristine AC, highlighting the enhanced degradation efficiency resulting from the synergistic integration of AC and TiO_2.

2. Experimental

2.1 Materials

Rice husk ash (RHA) was collected from a local source in Vietnam. Potassium hydroxide (KOH, ≥ 99%, China), sodium hydroxide (NaOH, ≥ 99.7%, China), titanium(IV) isopropoxide (TTIP, 97%, Sigma-Aldrich), isopropyl alcohol (≥ 99.8%, China), and ethanol (≥ 99.8%, China) were used as received without further purification. Basic Blue 3 (BB3, Sigma-Aldrich) was employed as the model organic dye in the photocatalytic degradation experiments.

2.2 Synthesis of TiO_2 nanoparticles

TiO_2 nanoparticles were synthesized via a sol–gel method using titanium(IV) isopropoxide (TTIP) as the precursor [21]. Briefly, 15 mL of TTIP was slowly added dropwise to 300 mL of isopropyl alcohol (IPA) under continuous magnetic stirring for 1 h to obtain a homogeneous precursor solution. Subsequently, a NaOH solution was added dropwise to adjust the pH to ~8 while stirring was maintained for another 1 h. The resulting suspension was centrifuged at 3500 rpm for 5 min to separate the precipitate, which was repeatedly washed with deionized water until the pH reached neutral (pH ≈ 7). The obtained solid was dried at 120°C for 1 h to remove residual solvents and then calcined at 500°C for 2 h to form crystalline TiO_2.

2.3 Synthesis of AC/TiO_2 nanocomposite

Rice husk ash-derived carbon (RHC) was first produced from rice husk ash (RHA) through KOH impregnation followed by drying, without undergoing a pyrolysis step. The obtained RHC was then converted into activated carbon (AC) through alkali activation using NaOH under ultrasonic assistance. This combined chemical–ultrasonic activation process promotes the development of a highly porous structure and increases accessible surface functionalities, consistent with previously reported activation strategies for biomass-derived carbons [22]. This approach was intended to reduce energy-intensive processing while still preserving the porous characteristics required for adsorption and photocatalytic applications.

The AC/TiO_2 nanocomposite was synthesized via a sol–gel process combining AC with the TTIP precursor. Specifically, 6.88 g of AC was dispersed in 137.6 mL of isopropyl alcohol containing 13.76 mL of TTIP, corresponding to the ratio of 1 g AC : 2 mL TTIP : 20 mL isopropyl alcohol [14]. The suspension was magnetically stirred for 1 h to ensure thorough penetration and uniform distribution of TTIP on the surface and within the porous structure of AC. The mixture was then dried at 120°C for 1 h and subsequently calcined at 500°C for 2 h to obtain the AC/TiO_2 nanocomposite.

2.4 Characterization

The crystalline structure of the samples was analyzed by X-ray diffraction (XRD) using a D8 Advance Eco diffractometer (Bruker, Germany) equipped with a Cu-Kα radiation source (λ = 1.5418 Å), operated at 40 kV and 25 mA with a scanning rate of $0.03°\cdot s^{-1}$. The morphology and elemental composition were examined using scanning electron microscopy coupled with energy-dispersive spectroscopy (SEM–EDS, JSM IT200, JEOL, Japan). Fourier-transform infrared (FT-IR) spectra were recorded on an iS50 FT-IR spectrometer (Nicolet, USA). The textural properties, including specific surface area and pore size distribution, were determined from N_2 adsorption–desorption isotherms measured at 77.3 K on a NOVA 1000e analyzer (Quantachrome, USA), applying the Brunauer–Emmett–Teller (BET) and Barrett–Joyner–Halenda (BJH) methods. The optical properties were investigated by UV–Vis spectroscopy in the range of 400 nm to 700 nm using a Jasco V-670 spectrophotometer (Jasco International Co., Japan). The by-products of photocatalytic degradation were identified using gas chromatography–mass spectrometry (GC–MS; GC: Agilent 6890 (g1350N), USA; MS: Agilent 5973 inert, USA).

2.5 Photocatalytic activity evaluation

Prior to the photocatalytic experiments, adsorption tests were conducted in the dark for 210 min to determine the adsorption–desorption equilibrium time. Photocatalytic degradation tests were then carried out to evaluate the removal of Basic Blue 3 (BB3) under UVC irradiation. The experiments were performed using a 20 ppm BB3 aqueous solution with a catalyst loading of 0.01 g per 100 mL solution, consistent with the adsorption conditions. The suspensions were magnetically stirred under a 15 W UVC lamp for 120 min. At 30 min intervals, 10 mL aliquots were withdrawn, centrifuged, and analyzed by UV–Vis spectroscopy to determine the temporal concentration changes. The adsorption efficiency (H, %) and photocatalytic efficiency were calculated using the following equation:

$$H\ (\%) = \frac{C_0 - C_t}{C_0} \times 100 \quad (1)$$

Where C_0 (ppm) is the initial concentration of BB3 and Ct (ppm) is the concentration at time t.

3. Results and discussion

3.1 Morphological, structural, and textural properties of photocatalysts

Figure 1 illustrates the surface morphology of annealed TiO_2 nanoparticles (a), activated carbon (b), and the AC/TiO_2 composite (c and d). As shown in Figure 1(a), the annealed TiO_2 exists a nearly spherical morphology as nanoparticles with diameters of approximately 500 nm, which tend to aggregate into larger clusters due to their high surface energy. Figure 1(b) reveals that the activated carbon exhibits a sheet-like morphology with stacked layers of irregular plates, each exceeding ~20 μm in size, providing a porous and rough texture. After the sol–gel process, the AC/TiO_2 composite (Figure 1(c,d)) shows TiO_2 nanoparticles randomly distributed both on the external surface

and within the interlayer space of AC. Compared to pristine TiO_2, the nanoparticles in the composite appear better dispersed and less aggregated, indicating that the AC framework not only acts as a supporting matrix but also suppresses excessive agglomeration.

The EDS mapping images of annealed TiO_2, activated carbon (AC), and the AC/TiO_2 composite are shown in Figures 2(a-c), respectively, while the elemental weight percentage distributions are presented in Figure 2(d). These results confirm the presence of the main elements Ti, O, and C, together with trace amounts of Mg and Ca. For the annealed TiO_2 sample, Ti (53.59 wt%) and O (44.80 wt%) were dominant, whereas C accounted for less than 2%. Activated carbon exhibited a composition rich in C (82.42 wt%) and O (14.78 wt%), with Ca and Mg present in small amounts (<2%). Notably, in the AC/TiO_2 composite, the coexistence of Ti (30.58 wt%), O (25.22 wt%), and C (44.20 wt%) demonstrates the successful distribution and attachment of TiO_2 on the AC surface.

Figure 3 shows the XRD patterns of annealed TiO_2, activated carbon, and the AC/TiO_2 composite. The annealed TiO_2 displays characteristic diffraction peaks of the anatase phase with a minor rutile signal, confirming its crystalline nature [23–25]. The average crystallite size of TiO_2 was estimated from the anatase (101) diffraction peak using the Scherrer equation, yielding a value of approximately 11.5 nm. It should be noted that this value corresponds to the crystallite size rather than the actual particle size. Activated carbon exhibits two broad peaks at around 25° and 43°, assigned to the (002) and (101) planes of amorphous carbon, consistent with previous studies [26–28]. For the AC/TiO_2 composite, the anatase peaks are still observed but with lower intensity, which can be ascribed to the amorphous background of AC and the good dispersion of TiO_2 on the carbon surface. This structural feature suggests that AC not only supports TiO_2 but also suppresses its crystal agglomeration, providing a favorable structure for photocatalytic and adsorption applications [29–31].

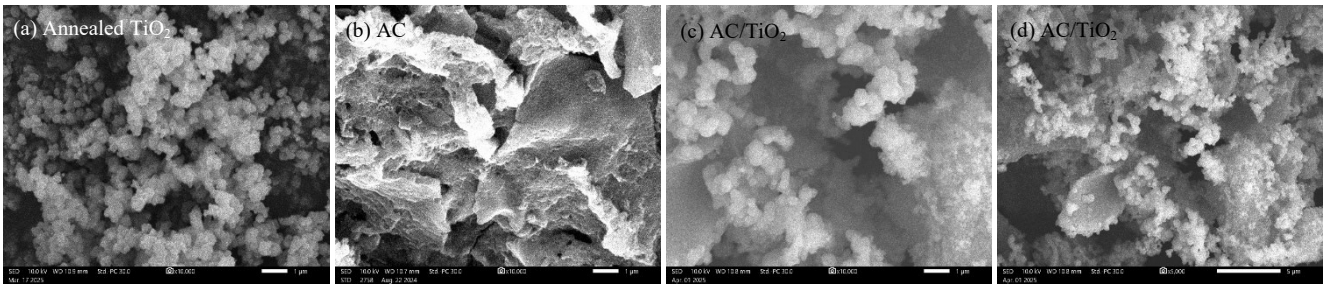

Figure 1. SEM images of annealed TiO_2 nanoparticles (a), activated carbon (b), and the AC/TiO_2 composite (c and d).

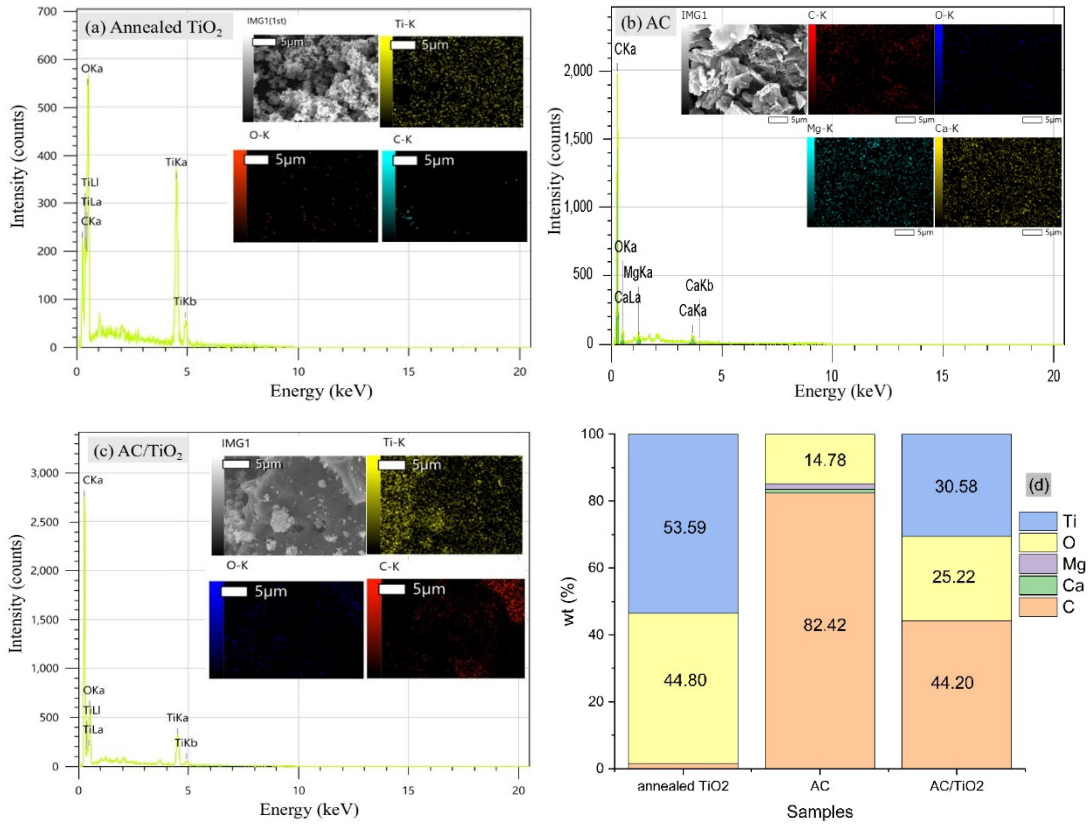

Figure 2. EDS spectra of annealed TiO_2 (a), activated carbon (b), and the AC/TiO_2 composite (c), together with the bar chart of elemental weight percentages in the samples (d).

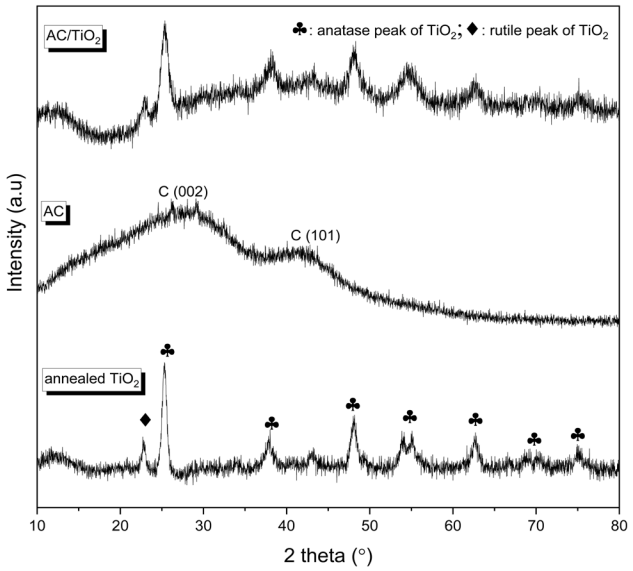

Figure 3. XRD pattern of annealed TiO_2, activated carbon, and the AC/TiO_2 composite.

Figure 4 presents the FT–IR spectra of annealed TiO_2, activated carbon, and the AC/TiO_2 composite. For annealed TiO_2, a broad absorption band in the range of 400 cm^{-1} to 700 cm^{-1} corresponds to Ti–O–Ti stretching vibrations, confirming the presence of TiO_2 lattice vibrations [32,33]. Activated carbon shows several characteristic peaks: a broad band around 3400 cm^{-1} assigned to the –OH stretching of surface hydroxyl groups, bands at 1700 cm^{-1} to 1600 cm^{-1} attributed to C=O and –COOH stretching vibrations, and weak absorptions in the region of 1200 cm^{-1} to 1000 cm^{-1} that can be associated with C–O functional groups [34,35]. In the AC/TiO_2 composite, the Ti–O–Ti band remains visible, while the intensity of the –OH and C=O bands is reduced compared to pristine AC. This shift and intensity change suggest interactions between TiO_2 nanoparticles and the functional groups on the AC surface, indicating chemical bonding or strong adsorption [36].

These findings are consistent with the XRD results, where the dispersion of TiO_2 on the amorphous carbon matrix was observed. Together, the XRD and FT–IR analyses confirm that AC not only acts as a support but also provides active functional groups that interact with TiO_2, leading to a more stable and synergistic composite structure [37].

The N_2 adsorption–desorption isotherms of activated carbon (AC) and the AC/TiO_2 composite are shown in Figure 5. Both samples exhibit hysteresis loops, indicating the presence of mesoporous structures and capillary condensation phenomena. The isotherms can be classified as type IV with an H4-type hysteresis loop, which is typically associated with slit-like pores commonly found in carbonaceous materials [38,39]. Activated carbon displays a much higher N_2 adsorption capacity compared with the composite, particularly at low relative pressures ($P/P_0 < 0.1$), which reflects the presence of abundant micropores. The pronounced H4 hysteresis loop around $P/P_0 \approx 0.4$ and the concave shape of the low-pressure region confirm a well-developed microporous network. The BET surface area of AC reaches approximately 887.3 $m^2 \cdot g^{-1}$, with a total pore volume of 0.337 $cm^3 \cdot g^{-1}$ and an average pore diameter of 3.46 nm, indicating a mixed micro–mesoporous structure.

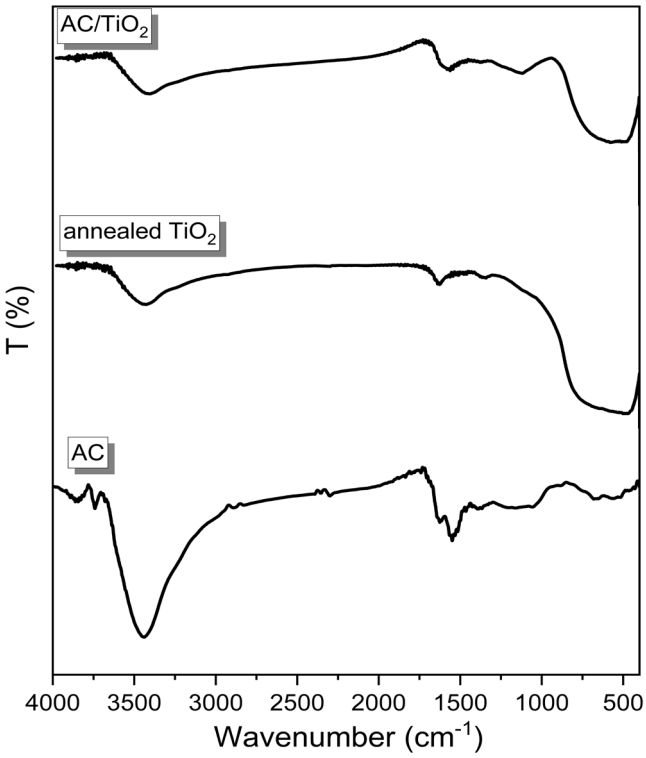

Figure 4. FT–IR spectrum of annealed TiO_2, activated carbon, and the AC/TiO_2 composite.

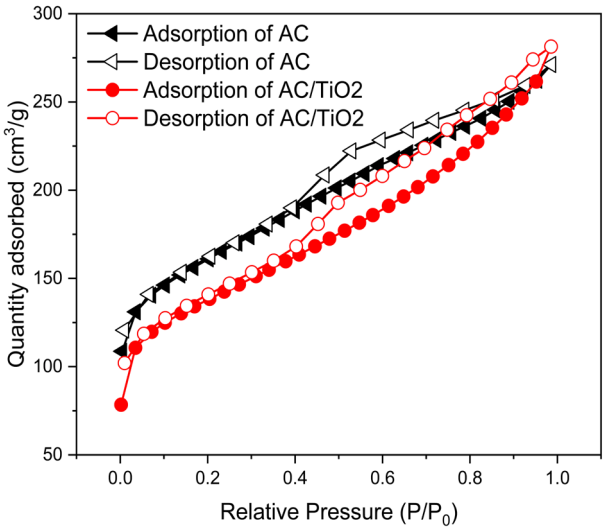

Figure 5: N_2 adsorption/desorption isotherms of AC and composite AC/TiO_2

For the AC/TiO_2 composite, the isotherm also shows an H4-type hysteresis, but with lower adsorption capacity and a narrower loop, suggesting that some pores of AC are blocked or partially filled by TiO_2 nanoparticles. The adsorption curve continues to rise toward higher relative pressures without reaching a clear plateau, implying that pore filling is not completely saturated and that interparticle voids or residual mesopores remain accessible to N_2 [40]. The BET surface area and total pore volume of the composite are reduced to 403.4 $m^2 \cdot g^{-1}$ and 0.241 $cm^3 \cdot g^{-1}$, respectively.The reduction in surface area and pore volume can be attributed to the TiO_2 nanoparticles

partially blocking the pores of activated carbon during high-temperature annealing (500°C). These results confirm that AC/TiO_2 maintains a hierarchical micro–mesoporous structure, where the micropores originate from the carbon framework and the interparticle voids are formed between TiO_2 particles anchored on the AC surface. Furthermore, the coexistence of micro- and mesoporous features in BET analysis is consistent with the XRD results, which confirmed the formation of crystalline TiO_2 phases well-dispersed on the carbon surface [41,42].

These textural features, together with the crystalline and surface chemistry results discussed earlier (XRD and FT-IR), confirm that TiO_2 nanoparticles are successfully integrated into the porous carbon framework, providing active sites while maintaining accessible porosity favorable for adsorption and photocatalytic processes.

3.2 Photocatalytic degradation performance of basic blue 3

The variation of basic blue3 (BB3, 20 ppm) dye concentration with time during adsorption over AC, AC/TiO_2, and annealed TiO_2 is shown in Figure 6. The results reveal that activated carbon (AC) exhibits the highest adsorption capacity due to its large specific surface area and well-developed microporous structure, consistent with the BET analysis. The BB3 concentration rapidly decreases within the first 30 min and reaches a nearly steady state after approximately 90 min, indicating that the adsorption–desorption equilibrium has been established. The strong adsorption ability of AC can be attributed to electrostatic attraction between negatively charged surface functional groups (–COOH, –OH) and cationic BB3 molecules, as well as π–π interactions between the aromatic rings of BB3 and the graphitic structure of AC [43].

In contrast, annealed TiO_2 shows negligible adsorption ability, as indicated by the almost constant C/C_0 ratio throughout the 210 min period. This is likely because the TiO_2 surface is mainly crystalline and lacks organic functional groups capable of dye adsorption. For the AC/TiO_2 composite, the BB3 concentration drops rapidly during the first 30 min and then stabilizes at a higher level than that of pure AC. This indicates that while the composite retains part of the adsorption capacity of the carbon matrix, the presence of TiO_2 nanoparticles reduces the effective surface area and partially blocks the pores, leading to lower overall adsorption capacity [44,45]. The equilibrium time of 90 min was thus selected to ensure that, in subsequent photocatalytic experiments, the decrease in BB3 concentration is solely due to photocatalytic degradation, not physical adsorption. After reaching adsorption–desorption equilibrium at 90 min, the samples were subsequently examined for their photocatalytic degradation performance of BB3 under light irradiation, as shown in Figure 7.

The photocatalytic degradation of basic blue 3 (BB3, 20 ppm) under UVC light (15 W) is illustrated in Figure 7. When no catalyst was used, the concentration of BB3 remained almost constant after 120 min of irradiation, indicating that UVC light alone was insufficient to induce significant photodegradation. For annealed TiO_2, no noticeable adsorption was observed in the dark ($C/C_0 \approx 1$). However, upon UVC illumination, the concentration ratio decreased to about 0.4 after 120 min, confirming the photocatalytic activation of TiO_2, where photogenerated electron–hole pairs lead to the formation of reactive oxygen species responsible for dye degradation. In contrast, AC primarily acted as an adsorbent rather than a photocatalyst. During the dark period, C/C_0 decreased to 0.19 due to dye adsorption on its surface, and only a slight further decrease to 0.13 was observed under UVC light, suggesting negligible photocatalytic activity.

Interestingly, the AC/TiO_2 composite exhibited a strong synergistic effect between adsorption and photocatalysis. In the dark, BB3 concentration reached equilibrium at $C/C_0 \approx 0.46$, and upon UVC exposure, it rapidly decreased to nearly zero, indicating complete discoloration. This superior performance can be attributed to the uniform dispersion of TiO_2 nanoparticles on the porous AC matrix, which enhances light absorption, electron transfer, and reduces recombination of photogenerated carriers. Therefore, among the tested materials, AC/TiO_2 demonstrated the highest photocatalytic efficiency, resulting from the combined effects of adsorption and photocatalytic degradation [46,47]. After confirming the photocatalytic activity of the catalysts, the effect of the initial BB3 concentration on the degradation efficiency under the same UVC irradiation conditions was further investigated, as shown in Figure 8.

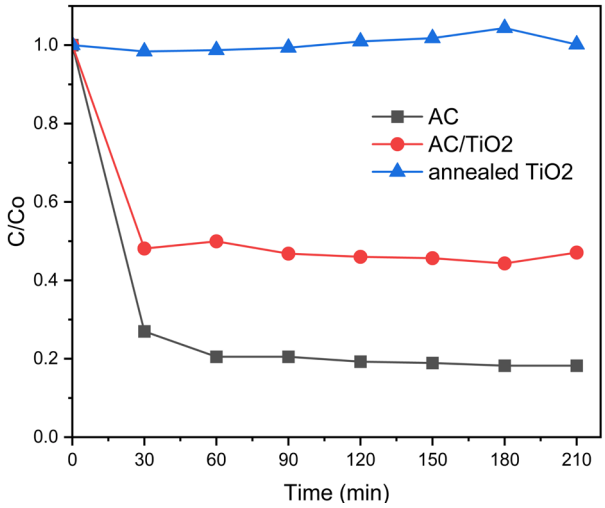

Figure 6: Variation of BB3 concentration over time during the adsorption process by AC, AC/TiO_2, and annealed TiO_2.

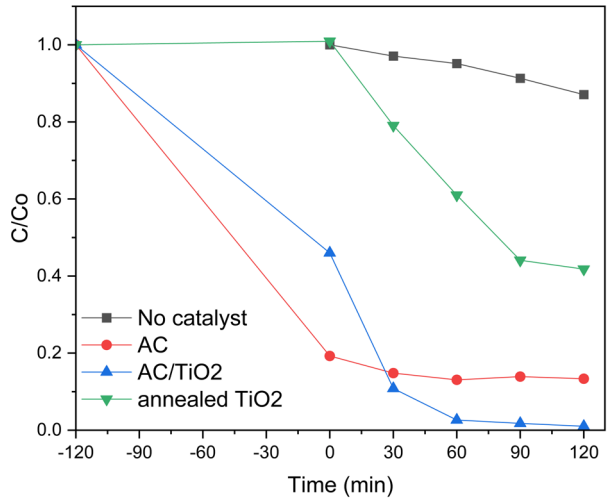

Figure 7: Variation of C/C_0 for BB3 solution (20 ppm) under 15 W UVC irradiation in the presence of different catalysts.

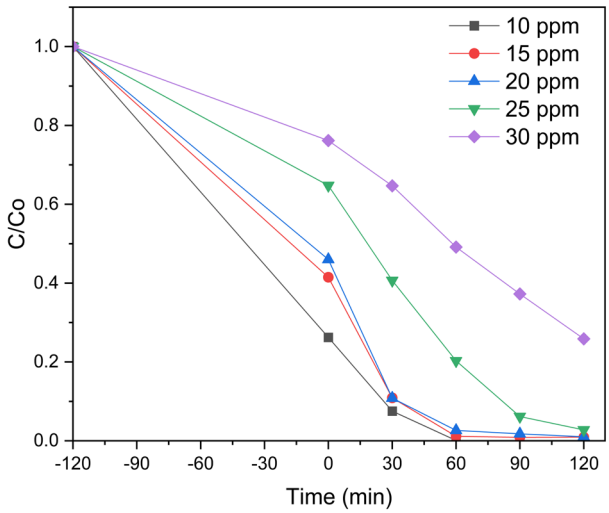

Figure 8: Photocatalytic degradation of BB3 solutions with different initial concentrations under UVC irradiation.

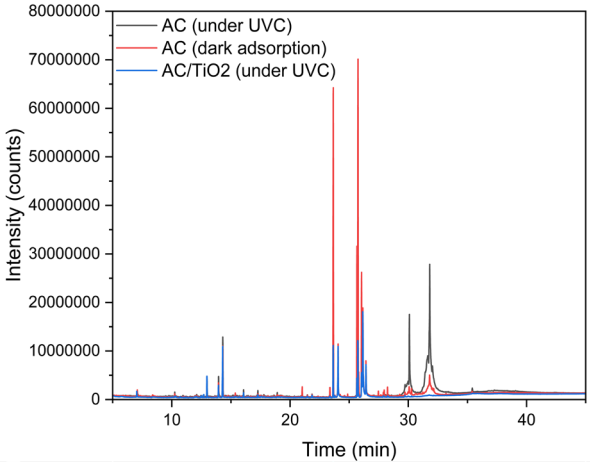

Figure 9: GC–MS chromatograms of BB3 solutions after treatment with AC (dark adsorption), AC under UVC irradiation, and AC/TiO_2 under UVC irradiation.

Figure 8 presents the photocatalytic degradation behavior of BB3 solutions with different initial concentrations (10 ppm to 30 ppm) under UVC irradiation. Before the UVC lamp was switched on ($t < 0$), the adsorption capacity of the AC/TiO_2 composite decreased with increasing initial BB3 concentration, indicating partial saturation of active sites on the catalyst surface. When the UVC lamp was turned on ($t \geq 0$), almost complete decolorization was achieved for solutions containing 10 ppm to 25 ppm BB3 within 60 min, whereas the degradation efficiency declined significantly at 30 ppm.

This phenomenon can be attributed to two main factors. First, at higher concentrations, the dense dye molecules compete for the limited active sites and light-generated reactive species ($^{\bullet}OH$, e^-/h^+), which suppresses photocatalytic efficiency [48,49]. Second, excessive dye molecules in the solution act as a light filter, absorbing and scattering UVC photons before they reach the catalyst surface. This reduces photon penetration and limits the excitation of TiO_2, thus decreasing the generation of oxidative radicals responsible for dye decomposition [50,51]. Consequently, the degradation rate is inversely related to the initial BB3 concentration when it exceeds the optimal range.

Although the overall color removal efficiency of AC and AC/TiO_2 for BB3 solution was nearly identical (approximately 100% after 120 min of UVC irradiation), the underlying mechanisms responsible for this effect differ significantly. In the case of AC, the decrease in BB3 concentration mainly results from physical adsorption of dye molecules onto the activated carbon surface. Conversely, the AC/TiO_2 composite exhibits a strong photocatalytic degradation capability in addition to initial adsorption, owing to the catalytic activity of TiO_2. To verify this distinction and elucidate the degradation pathway, GC–MS analysis was conducted to identify the intermediate species generated after the photocatalytic process. The GC–MS results provide direct evidence of BB3 molecular fragmentation under UVC irradiation, confirming that the color removal observed for AC/TiO_2 arises from true photocatalytic degradation rather than mere adsorption.

The GC–MS results in Figure 9 reveal pronounced differences among BB3 solutions treated with AC in the dark, AC under UVC illumination, and AC/TiO_2 under UVC illumination. The chromatogram of the dark-adsorbed AC sample exhibits several high-intensity peaks at retention times of 22 min to 30 min, corresponding to medium (m/z 120 to 260) and large (m/z 300 to 356) ions [52]. This indicates that the BB3 molecules largely remain intact, consistent with a purely adsorption-based process without chemical bond cleavage. Similarly, the AC sample under UVC irradiation still shows prominent peaks, albeit with slightly reduced intensities, demonstrating that 15 W UVC radiation alone is insufficient to degrade BB3—an observation aligned with the nearly unchanged BB3 concentration in Figure 7.

Although UVC irradiation demonstrated effective activation of the AC/TiO_2 composite in the present study, its practical application may be constrained by limited penetration depth and the absence of natural UVC irradiation in sunlight. Nevertheless, low-power UVC sources remain useful for controlled laboratory-scale evaluation of intrinsic photocatalytic activity and may offer additional advantages in combined pollutant degradation–disinfection systems due to their well-known germicidal properties.

In contrast, the AC/TiO_2–UVC sample displays a markedly altered chromatographic pattern: the characteristic high-intensity peaks of intact BB3 nearly disappear, replaced by multiple low-intensity peaks at shorter retention times (10 min to 20 min) corresponding to low-mass ions (m/z 43 to 75) and some medium-mass fragments [52,53]. The appearance of such smaller species confirms that AC/TiO_2 induces true photocatalytic breakdown of BB3, leading to fragmentation of its anthraquinone–azo structure. Therefore, although AC and AC/TiO_2 exhibit similar overall discoloration efficiencies in Figure 7, GC–MS conclusively shows that their mechanisms are fundamentally different: AC removes color via adsorption, while AC/TiO_2 genuinely decomposes BB3 into smaller intermediates.

The presence of low-m/z fragments in the AC/TiO_2 sample highlights the involvement of strong oxidative species generated during photocatalysis. Upon UVC irradiation, TiO_2 produces electron–hole pairs (e^-/h^+). Holes (h^+) oxidize surface-bound H_2O or OH^- to form hydroxyl radicals ($^{\bullet}OH$), while electrons (e^-) reduce dissolved oxygen to $^{\bullet}O_2^-$. These reactive species attack the anthraquinone backbone, the azo bond (–N=N–), and aromatic rings of BB3, leading to fragmentation and the formation of low-mass intermediates observed in GC–MS. The AC support further enhances BB3 adsorption, TiO_2 dispersion, and charge separation, thereby promoting more efficient photocatalytic

degradation. BB3 possesses a characteristic anthraquinone–azo framework. The expected degradation pathway includes: (i) Azo bond cleavage (–N=N–), yielding two intermediate fragments with medium m/z (120 to 260); (ii) $^{\bullet}OH$ attack on the anthraquinone ring, forming hydroxylated derivatives followed by ring-opening, (iii) Cleavage of alkyl/amine substituents, producing low-m/z fragments (43 to 75), (iv) Partial mineralization into small organic acids, aniline derivatives, or low-mass quinone fragments [52,54,55].

Photocatalytic evaluation demonstrates that AC/TiO_2 exhibits substantially higher degradation activity toward BB3 compared to AC or TiO_2 alone. Whereas AC removes color mainly by adsorption, AC/TiO_2 not only adsorbs but also decomposes BB3 into smaller molecules under UVC irradiation, as confirmed by the disappearance of BB3 peaks in the GC–MS spectra. The degradation efficiency decreases at higher BB3 concentrations due to surface saturation and reduced photon penetration.

Although the present study confirms the photocatalytic degradation capability of the synthesized AC/TiO_2 composite through GC–MS analysis, further investigations involving kinetic modeling, scavenger-assisted radical identification, and catalyst reusability tests are still necessary to establish a more comprehensive mechanistic understanding.

4. Conclusions

In this study, the AC/TiO_2 composite was demonstrated to be an effective material for the removal of BB3 through the combined actions of adsorption and photocatalytic degradation. The composite preserves the high surface area of activated carbon while incorporating the strong reactive-species–generating capability of TiO_2, resulting in significantly enhanced removal efficiency compared to pristine AC. GC–MS analysis provided direct evidence that AC removes the dye solely via adsorption, whereas AC/TiO_2 induces molecular fragmentation, producing multiple low–molecular-weight intermediates consistent with oxidative attack by $^{\bullet}OH$, h^+, a nd e^- species. Overall, AC/TiO_2 represents a highly promising material for dye-contaminated wastewater treatment owing to its efficiency, stability, and well-defined degradation mechanism. The present work highlights a relatively mild and energy-saving activation strategy for preparing porous AC/TiO_2 composites from rice husk ash without conventional pyrolysis treatment. These findings establish a basis for future work on material optimization, extension to other recalcitrant organics, and evaluation under real environmental conditions. Future work will focus on detailed photocatalytic kinetic analysis, radical trapping experiments, optimization of operational parameters, and long-term catalyst stability evaluation.

Acknowledgements

This research is funded by Vietnam National University, Ho Chi Minh City (VNU-HCM) under grant number C2025-18-27.

References

[1] W. Promsuwan, P. Sujaridworakun, and W. Reainthippayasakul, “Synthesis of zinc oxide photocatalysts from zinc-dust waste for organic dye degradation,” *Journal of Metals, Materials and Minerals*, vol. 33, no. 2, pp. 58–64, 2023.

[2] G. Wongwaen, K. Dechsri, P. Opanasopit, M. Aiempanakit, and C. Suwanchawalit, “Sulfur-doped carbon dots derived from caffeine: A highly efficient photocatalyst for organic dye degradation,” *Journal of Metals, Materials and Minerals*, vol. 35, no. 4, p. 2355, 2025.

[3] E. O. Alegbea, and T. O. Uthman, "A review of history, properties, classification, applications and challenges of natural and synthetic dyes," *Heliyon*, vol. 10, no. 13, p. e33646, 2024.

[4] D. A. Yaseen, and M. Scholz, "Textile dye wastewater characteristics and constituents of synthetic effluents: A critical review," *International Journal of Environmental Science and Technology*, vol. 16, no. 2, pp. 1193–1226, 2019.

[5] G. Crini, "Recent developments in polysaccharide-based materials used as adsorbents in wastewater treatment," *Progress in Polymer Science*, vol. 30, pp. 38–70, 2005.

[6] G. Crini, and E. Lichtfous, “*Green Adsorbents for Pollutant Removal*, Environmental Chemistry for a Sustainable World 18, Springer, pp. 23–71, 2019.

[7] P. Norranattrakul, K. Siralertmukul, and R. Nuisin, “Fabrication of chitosan/titanium dioxide composites film for the photocatalytic degradation of dye”, *Journal of Metals, Materials and Minerals*, vol. 23, no. 2, pp. 9–22, 2013.

[8] M. Pelaez, N. T. Nolan, S. C. Pillai, M. K. Seery, P. Falaras, A. G. Kontos, P. S. M. Dunlop, J. W. J. Hamilton, J. A. Byrne, K. O'Shea, M. H. Entezari, and D. D. Dionysiou, "A review on the visible light active titanium dioxide photocatalysts for environmental applications," *Applied Catalysis B: Environmental*, vol. 125, pp. 331–349, 2012.

[9] S. Tanigawa, T. Takashima, and H. Irie, "Enhanced visible-light-sensitive two-step overall water-splitting based on band structure controls of titanium dioxide and strontium titanate," *Journal of Materials Science and Chemical Engineering*, vol. 5, no. 1, 2017.

[10] J. Schneider, M. Matsuoka, M. Takeuchi, J. Zhang, Y. Horiuchi, M. Anpo, and D. W. Bahnemann, "Understanding TiO_2 photocatalysis: Mechanisms and materials," *Chemical* Reviews, vol. 114, no. 19, pp. 9919–9986, 2014.

[11] X. Chen, and S. S. Mao, "Titanium dioxide nanomaterials: synthesis, properties, modifications, and applications," *Chemical Reviews*, vol. 107, no. 7, pp. 2891–2959, 2007.

[12] B. Zhou, Z. Zhang, Y. Li, G. Han, Y. Feng, B. Wang, D. Zhang, J. Ma, and C. Liu, "Flexible, Robust, and multifunctional electromagnetic interference shielding film with alternating cellulose nanofiber and MXene layers," *ACS Applied Materials & Interfaces*, vol. 12, no. 4, pp. 4895–4905, 2020.

[13] X. Hu, L. Xiao, X. Jian, and W. Zhou, "Synthesis of mesoporous silica-embedded TiO_2 loaded with Ag nanoparticles for photocatalytic hydrogen evolution from water splitting," *Journal of Wuhan University of Technology – Materials Science Edition*, vol. 32, pp. 67–75, 2017.

[14] C. W. Kartikowati, A. L. Wulansari, B. P. Poerwadi, S. Super, A. F. Arif, T. Sulistyaningsih, and O. Arutanti, "TiO_2/AC composites for adsorption–photocatalytic of methyl orange," *IOP Conference Series: Materials Science and Engineering*, vol. 1143, 012077, 2021.

[15] M. R. Meirelles, A. S. Giroto, K. Furukawa, and M. Gonçalves, "Valorization of lignocellulosic biomass for photocatalytic

applications: Development of activated carbon–TiO_2 composites," *ACS Sustainable Resource Management*, vol. 2, no. 3, pp. 524–535, 2025.

[16] S. J. Armaković, and S. Armaković, "Zeolite-Supported TiO_2 for enhanced photocatalytic performance in environmental applications: A review," *Catalysts*, vol. 15, no. 2, p. 174, 2025.

[17] F. Dalto, I. Kuźniarska-Biernacka, C. Pereira, E. Mesquita, O. S. G. P. Soares, M. F. R. Pereira, M. J. Rosa, A. S. Mestre, A. P. Carvalho, and C. Freire, "Solar Light-induced methylene blue removal over TiO_2/AC composites and photocatalytic regeneration," *Nanomaterials*, vol. 11, no. 11, 3016, 2021.

[18] Y. M. Adib, Z. Al-Qodah, and C. W. Z. Ngah, "Agricultural bio-waste materials as potential sustainable precursors used for activated carbon production: A review," *Renewable and Sustainable Energy Reviews*, vol. 46, pp. 218–235, 2015.

[19] V. N. Ullal, S. H. T, and A. K. P, "Rice husk ash utilization, composition and properties: A brief review", *Journal of Metals, Materials and Minerals*, vol. 32, no. 4, pp. 37–46, 2022.

[20] N. A. C. Imani, W. D. P. Rengga, W. B. Sediawan, H. H., and K. A. Salsabiil, "Adsorption studies of rice husk-based silica/carbon composite," *EKSAKTA Journal of Sciences and Data Analysis*, vol. 1, no. 2, pp. 98–104, 2020.

[21] J. Morales, A. Maldonado, and M. de la L. Olvera, "Synthesis and characterization and photocatalytic activity of TiO_2 powders," *13th International Conference on Electrical Engineering, Computing Science and Automatic Control (CCE)*, 2016.

[22] M. S. Yerdauletov, K. Nazarov, B. Mukhametuly, M. A. Yeleuov, C. Daulbayev, R. Abdulkarimova, A. Yskakov, F. Napolskiy, and V. Krivchenko, "Characterization of activated carbon from rice husk for enhanced energy storage devices," *Molecules*, vol. 28, no. 15, p. 5818, 2023.

[23] M. M. Ahmad, S. Mushtaq, H. S. Al Qahtani, A. Sedky, and M. W. Alam, "Investigation of TiO_2 nanoparticles synthesized by sol-gel method for effectual photodegradation, oxidation and reduction reaction," *Crystals*, vol. 11, no. 12, p. 1456, 2021.

[24] A. K. John, S. Palatty, and S. S. Sharma, "Greener approach towards the synthesis of titanium dioxide nanostructures with exposed {001} facets for enhanced visible light photodegradation of organic pollutants," *Journal of Materials Science: Materials in Electronics*, vol. 31, no. 3, pp. 1–15, 2020.

[25] G. Nagaraj, D. Brundha, C. Chandraleka, M. Arulpriya, V. Kowsalya, S. Sangavi, R. Jayalakshmi, S. Tamilarasu, and R. Murugan, "Facile synthesis of improved anatase TiO_2 nanoparticles for enhanced solar-light driven photocatalyst," *SN Applied Sciences*, vol. 2, p. 734, 2020

[26] Y.-J. Heo, and S.-J. Park, "Synthesis of activated carbon derived from rice husks for improving hydrogen storage capacity," *Journal of Industrial and Engineering Chemistry*, vol. 31, pp. 330–334, 2015.

[27] H. Kulkarni, C. Bari, S. Mukherjee, P. Gajera, and G. Sethia, "Waste biomass-derived activated carbons for selective oxygen adsorption," *Carbon Trends*, vol. 17, p. 100398, 2024.

[28] N. A. Negm, A. A. Altalhi, H. M. Ahmed, and E. A. Mohamed, "Synergistic effect of rice husk-derived activated carbon modified by Ni/Al-layered double hydroxides for lead removal from industrial wastewater," *Scientific Reports*, vol. 14, p. 28411, 2024.

[29] Y. Yue, X. Yue, X. Tang, L. Han, J. Wang, S. Wang, and C. Du, "Synergistic adsorption and photocatalysis study of TiO_2 and activated carbon composite," *Heliyon*, vol. 10, no. 10, p. e30817, 2024.

[30] M. Peñas-Garzón, A. Gómez-Avilés, J. Bedia, J. J. Rodriguez, and C. Belver, "Effect of activating agent on the properties of TiO_2/activated carbon heterostructures for solar photocatalytic degradation of acetaminophen," *Materials*, vol. 12, no. 3, p. 378, 2019.

[31] M. Chobchun, P. Jutakridsada, P. Thiamsinsangwon, P. Kasemsiri, and K. Kamwilaisak, "Characterization of TiO_2-activated carbon onto adsorption and photocatalytic properties and its application," *Journal of Metals, Materials and Minerals*, vol. 30, no. 4, Art. no. 3, 2020.

[32] M. Chobchun, P. Jutakridsada, P. Thiamsinsangwon, P. Kasemsiri, K. Kamwilaisak, and P. Chindaprasirt, "Characterization of TiO_2-activated carbon onto adsorption and photocatalytic properties and its application", *Journal of Metals, Materials and Minerals*, vol. 30, no. 4, pp. 30–38, 2020.

[33] A. León, P. Reuquen, C. Garín, R. Segura, P. Vargas, P. Zapata, and P. A. Orihuela, "FTIR and raman characterization of TiO_2 nanoparticles coated with polyethylene glycol as carrier for 2-methoxyestradiol," *Applied Sciences*, vol. 7, no. 1, p. 49, 2017.

[34] K. Kitsanadecha, C. Sinmak, P. Onchomchan, K. Hantana-sirisakul, T. Kwamman, and S. Anantachaisilp, "Synthesis and characterization of electron beam irradiated glutinous rice husk-derived biochar and activated carbon for aqueous electrochemical capacitors", *Journal of Metals, Materials and Minerals*, vol. 33, no. 3, p. 1687, 2023.

[35] O. A. Hussain, A. S. Hathout, Y. E. Abdel-Mobdy, M. M. Rashed, and E. A. Abdel Rahim, "Preparation and characterization of activated carbon from agricultural wastes and their ability to remove chlorpyrifos from water," *Toxicology Reports*, vol. 10, pp. 146–154, 2023.

[36] C. Parvathiraja, S. Katheria, M. R. Siddiqui, S. M. Wabaidur, M. A. Islam, and W.-C. Lai, "Activated carbon-loaded titanium dioxide nanoparticles and their photocatalytic and antibacterial investigations," *Catalysts*, vol. 12, no. 8, p. 834, 2022.

[37] W. Liu, B. Wang, and M. Zhang, "Effect of process parameters on the microstructure and performance of TiO_2-loaded activated carbon," *ACS Omega*, vol. 6, no. 50, pp. 35076–35092, 2021.

[38] M. R. Meirelles, A. S. Giroto, K. Furukawa, and M. Gonçalves, "Valorization of lignocellulosic biomass for photocatalytic applications: development of activated carbon–TiO_2 composites," *ACS Sustainable Resource Management*, vol. 2, no. 3, pp. 524–535, 2025.

[39] O. Arutanti, A. L. Sari, C. W. Kartikowati, A. A. Sari, and A. F. Arif, "Design and application of homogeneous-structured TiO_2/activated carbon nanocomposite for adsorption–photocatalytic degradation of MO," *Water, Air, and Soil Pollution*, vol. 233, no. 4, p. 118, 2022.

[40] E. M. el Mountassir, L. El Mersly, K. Belkodia, A. Piram, S. Lebarillier, S. Briche, S. Rafqah, and P. Wong-Wah-Chung, "Sol-gel synthesis of new TiO_2 ball/activated carbon photocatalyst and its application for degradation of three hormones: 17α-ethinylestradiol, estrone, and β-estradiol," *Toxics*, vol. 11, no. 4, p. 299, 2023.

[41] A. Zawawi, R. M. Ramli, and N. Y. Harun, "Synergistic effect of adsorption-photodegradation of composite TiO_2/AC for degradation of 1-butyl-3-methylimidazolium chloride," *Malaysian Journal of Analytical Sciences*, vol. 22, no. 4, pp. 648–658, 2018.

[42] M. Chobchun, P. Jutakridsada, P. Thiamsinsangwon, P. Kasemsiri, K. Kamwilaisak, and P. Chindaprasirt, "Characterization of TiO_2-activated carbon onto adsorption and photocatalytic properties and its application," *Journal of Metals, Materials and Minerals*, vol. 30, no. 4, pp. 30–38, 2020.

[43] T. B. Budak, "Adsorption of basic yellow 28 and basic blue 3 dyes from aqueous solution using silybum marianum stem as a low-cost adsorbent," *Molecules*, vol. 28, no. 18, p. 6639, 2023.

[44] C. Boonwan, T. Rojviroon, O. Rojviroon, R. Rajendran, S. Paramasivam, R. Chinnasamy, S. Ansar, and S. Boonyuen, "Micro-nano bubbles in action: AC/TiO_2 hybrid photocatalysts for efficient organic pollutant degradation and antibacterial activity," *Biocatalysis and Agricultural Biotechnology*, vol. 61, p. 103400, 2024.

[45] Y. Li, Q. Shen, R. Guan, J. Xue, X. Liu, H. Jia, B. Xu, and Y. Wu, "AC@TiO_2 yolk–shell heterostructure for synchronous photothermal–photocatalytic degradation of organic pollutants," *Journal of Materials Chemistry C*, vol. 8, pp. 1025–1040, 2020.

[46] Y. L. Pang, S. Lim, and R. K. L. Lee, "Enhancement of sonocatalytic degradation of organic dye by using titanium dioxide (TiO_2)/activated carbon (AC) derived from oil palm empty fruit bunch," *Environmental Science and Pollution Research*, vol. 27, pp. 34638–34652, 2020.

[47] S. N. Saeedi, M. H. Rasoulifard, M. S. S. Dorraji, H. Douroudgari, and N. Sehati, "Enhanced photocatalytic degradation of organic pollutants using a TiO_2–clay nanocomposite in a rotary photoreactor with experimental and theoretical insights," *Scientific Reports*, vol. 15, p. 38193, 2025.

[48] B. Mondol, A. Sarker, A. M. Shareque, S. C. Dey, M. T. Islam, A. K. Das, S. M. Shamsuddin, M. A. I. Molla, and M. Sarker, "Preparation of activated carbon/TiO_2 nanohybrids for photodegradation of reactive red-35 dye using sunlight," *Photochem*, vol. 1, no. 1, pp. 54–66, 2021.

[49] S. Jaybhaye, N. Shinde, S. Jaybhaye, and H. Narayan, "Photocatalytic degradation of organic dyes using titanium dioxide (TiO_2) and Mg-TiO_2 nanoparticles," *Journal of Nanotechnology and Nanomaterials*, vol. 3, no. 2, pp. 67–76, 2022.

[50] N. Ramesh, C. W. Lai, M. R. Johan, S. M. Mousavi, I. A. Badruddin, A. Kumar, G. Sharma, and F. Gapsari, "Progress in photocatalytic degradation of industrial organic dye by utilising the silver doped titanium dioxide nanocomposite," *Heliyon*, vol. 10, no. 24, p. e40998, 2024.

[51] A. Ajmal, I. Majeed, R. N. Malik, H. Idriss, and M. A. Nadeem, "Principles and mechanisms of photocatalytic dye degradation on TiO_2 based photocatalysts: A comparative overview," *RSC Advances*, vol. 4, pp. 37003–37026, 2014.

[52] A. R. Khataee, M. Fathinia, S. Aber, and M. Zarei, "Optimization of photocatalytic treatment of dye solution on supported TiO_2 nanoparticles by central composite design: Intermediates identification," *Journal of Hazardous Materials*, vol. 181, pp. 886–897, 2010.

[53 U. U. Rahman, A. Khan, A. Asadullah, M. Humayun, N. Shah, A. F. Alanazi, and M. Bououdina, "Copper-modified graphene oxide and reduced graphene oxide nanocomposites for the photo-assisted removal of basic blue-3 dye," *RSC Advances*, vol. 15, pp. 29034–29052, 2025.

[54] M. Fathinia, A. R. Khataee, M. Zarei, and S. Aber, "Comparative photocatalytic degradation of two dyes on immobilized TiO_2 nanoparticles: Effect of dye molecular structure and response surface approach," *Journal of Molecular Catalysis A: Chemical*, vol. 333, pp. 73–84, 2010

[55] A. Khataee, M. Taseidifar, M. Sheydaei, S. Khorram, and S. W. Joo, "Sonocatalytic degradation of basic blue 3 using plasma-treated magnetite nanostructures," *Current Nanoscience*, vol. 12, no. 1, pp. 125–134, 2016.